ADVANCED OPTICAL MATERIALS
www.advopticalmat.de

# Ultrafast Electro-Absorption Switching in Colloidal CdSe/CdS Core/Shell Quantum Dots Driven by Intense THz Pulses

*Claudia Gollner,* Rokas Jutas, Dominik Kreil, Dmitry N. Dirin, Simon C. Boehme, Andrius Baltuška, Maksym V. Kovalenko, and Audrius Pugžlys**

**Next-generation high-speed optical networks demand the development of ultrafast optical interconnects capable of Tbit $s^{-1}$ data rates. By utilizing colloidal CdSe/CdS core/shell quantum dots, gated by intense THz pulses, a proof of concept of an all-optical femtosecond electro-absorption switch is presented in this work. Without any additional enhancement of the THz electric field, an extinction contrast of more than 6 dB and transmission changes in the visible of more than 15% are achieved, with the latter setting a new record for solution-processed electro-absorption materials at room temperature. The absence of physical artifacts, originating from electrodes and field enhancing structures, allows to employ a simple and intuitive numerical model, which rationalizes the large field-induced electro-absorption response. Supported by theoretical calculations, the importance of the energy band alignment of heterostructure quantum dots are discussed for the first time and suggest that further improvement of the modulation depth and contrast may be achieved with Type-II quantum dots.**

## 1. Introduction

Rapidly developing modern optical communication systems demand small-scale electro-optic devices with large and fast changes in optical properties. Such nanoscale devices can be used, for example, as optical interconnects for data-storage or on-chip data links.[1] Over the past few decades, a particularly promising role in high-speed optical networks has been suggested for electro-absorption (EA) modulators based on quantum-well structures.[2,3] Utilizing the quantum confined Stark effect (QCSE), the optical properties of these materials can be modulated via an external electric field along the confinement axis, that is, via skewing the potential well. As a consequence of such "tilted" valence and conduction bands, the associated lowest energy electron and hole wavefunctions will localize at opposite sides of the potential well, hereby leading to a modification of the absorption spectrum in the vicinity of the band gap. Typical signatures of such a field-induced modulation are a reduced overlap integral between the wavefunctions, a reduced oscillator strength of the associated optical transitions and a decreased transition energy which is manifested in a red shifted absorption edge.[4–6]

State-of-the-art EA modulators based on the QCSE mainly consist of epitaxially grown multiple quantum-well structures with a maximum bandwidth of 23 GHz,[7] data rates of 40 Gb $s^{-1}$,[8] and extinction ratio of 10 dB. The modulation speed and signal contrast in such modulators is fundamentally limited by the time scale necessary to change the electric field and the optimization of the RF electrodes, respectively.[9] In addition, the extent to which the quantum states can be manipulated by increasing the AC electric field strength is limited by the dielectric breakdown of the material. Naturally, a route to overcome these physical limits is to use high frequency THz wave-forms as a driving field, to implement a Tbit $s^{-1}$ system[10] whilst avoiding dielectric breakdown owing to the low duty cycle. Moreover, largest modulation of the energy levels can be achieved for structures with a strong confinement resulting in large exciton binding energies, leading to sharp absorption features. Such prominent peaks can translate to large changes in absorption, even for small energy shifts. Therefore,

C. Gollner, R. Jutas, A. Baltuška, A. Pugžlys
Photonics Institute
TU Wien
Gusshausstrasse 27-29/387, Vienna A-1040, Austria
E-mail: claudia.gollner@tuwien.ac.at; audrius.pugzlys@tuwien.ac.at
D. Kreil
Institute for Theoretical Physics
Johannes Kepler University
Altenbergerstraße 69, Linz A-4040, Austria
D. N. Dirin, S. C. Boehme, M. V. Kovalenko
Institute of Inorganic Chemistry
Department of Chemistry and Applied Bioscience, ETH Zürich
Vladimir Prelog Weg 1, Zürich CH-8093, Switzerland
D. N. Dirin, S. C. Boehme, A. Baltuška, M. V. Kovalenko
Empa-Swiss Federal Laboratories for Materials Science and Technology
Überlandstrasse 129, Dübendorf CH-8600, Switzerland
A. Pugžlys
Center for Physical Sciences & Technology
Savanoriu Ave. 231, Vilnius LT-02300, Lithuania
The ORCID identification number(s) for the author(s) of this article can be found under https://doi.org/10.1002/adom.202102407.



**DOI: 10.1002/adom.202102407**

low-dimensional materials like quantum dots (QDs) are promising candidates for EA modulators.

In a pioneering work,[11] Hoffmann and coworkers reported on sup-ps optical absorption switching in an InGaAs/GaAs QD-based saturable absorber mirror, induced by an incident THz pulse. A few years later, Pein et al.[12,13] demonstrated THz-field induced QCSE in CdSe/CdS colloidal QDs. However, due to difficulties to generate THz radiation with an electric field strength in the MV $cm^{-1}$ range, necessary to alter the QD band gap and to change the optical transmission, a micro-slit array consisting of parallel gold lines was employed as a THz field enhancing structure. Consequently, the resulting THz field is inhomogeneous and additional processes, such as electrode driven charge injection, cannot be entirely decoupled from the QCSE, introducing systematic errors in the description of the underlying physical mechanisms. To date, generation of intense THz pulses with large electric field amplitudes in the MV $cm^{-1}$ range becomes more and more feasible,[14–18] which allows on-demand control of the properties of matter.

In this work, to the best of our knowledge, we report for the first time on a direct all optical encoding of a free space THz signal onto an optical probe signal in semiconductor QDs without any field enhancing structures. This simple approach reveals several advantages. First, the possibility to manipulate optical properties of nano-scale semiconductors by direct THz radiation significantly simplifies the experimental setup and device design, opens new perspectives in studying THz induced QCSE in a large variety of samples and excludes possible artifacts introduced by field enhancing structures. Second, experiments can be performed on colloidal CdSe/CdS core/shell QDs, which allows for facile solution processing of the EA material. The achieved change in absorption exceeds 15% when the short THz pulse and sub-50 fs optical probe temporally overlap, outperforming previously reported modulators based on solution processed materials.[19] Furthermore, we investigate the interplay between the spectral bandwidth and pulse duration of the probe pulse with respect to the modulation contrast and demonstrate that by controlling the THz waveform, an extinction ratio of more than 6 dB can be achieved, which is on a par with state-of-the-art epitaxial quantum-well EA modulators. Because the energy band structure acts on the EA modulation efficiency,[20] we employ a simple theoretical model which matches the experimental data remarkably well and identifies the most suitable energy band alignment. The results demonstrate a possibility for high speed optical communication systems with Tbit $s^{-1}$ data rates and suggest a route to optimize EA modulation by band gap engineering of colloidal QDs.

## 2. Results and Discussion

### 2.1. Sample Preparation and Characterization

The CdSe/CdS core/shell QDs are synthesized following the well established procedure described by Chen et al.[21] with minor modifications. Details on the synthesis method can be found in the Supporting Information (Section S1). Essential in this procedure is that the high-temperature injection of trioctylphosphine selenide (TOPSe) and the chosen ligands octadecylphosphonate (ODPA) allow to make a wurtzite CdSe core. In combination with a slow shell growth using hexanethiol, highly uniform shell coating is enabled and secondary nucleation of CdS QDs is prevented. The resulting QDs consist of a CdSe core with an average diameter of 4.1 nm and a CdS shell with a thickness of 2.4 nm. A transmission electron microscopy (TEM) image is shown in Figure S1 in Supporting Information, revealing a size distribution of 8.9 ± 0.8 nm in diameter. The colloidal QDs are deposited on a glass substrate by simple drop casting, forming a thin film of limited homogeneity (see inset of Figure S1b, Supporting Information).

**Figure 1**a displays the absorption spectrum, measured with a UV–Vis–NIR spectrophotometer (Cary 5G) (blue dots), and a fit (red line) consisting of multiple Gaussian components and a polynomial cubic background term describing the absorption continuum[22,23] (green dashed lines). The red side (edge) of the absorption spectrum of the CdSe/CdS QD film is dominated by two lowest-energy transitions denoted as $X_1$ and $X_2$, corresponding to the transitions $1S_{3/2}(h) \rightarrow 1S(e)$ and

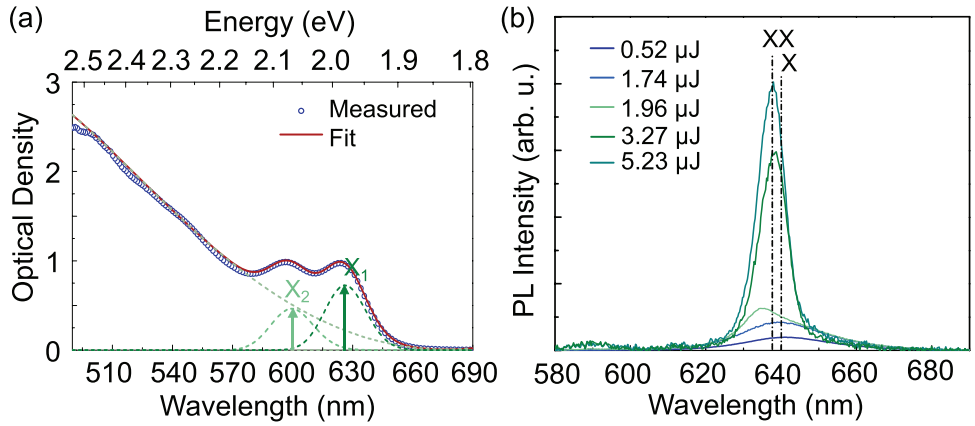


**Figure 1.** a) Measured optical density of the QD film (blue dots) and fit function (red line). The green dashed lines present the decomposed fit function consisting of a cubic background and two discrete Gaussian energy transitions ($X_1$ and $X_2$). b) Photoluminescence spectrum when the QD film is excited with 515 nm pulses of different energies (see legend). At low excitation energy, the exciton emission is centered at 640 nm. At higher pump energies, a second peak appears at slightly higher photon energies, which corresponds to biexciton emission, implying a quasi Type II band structure.

$2S_{3/2}(h) \rightarrow 1S(e)$, respectively, labeled by a principal quantum number, an angular momentum state and a total angular momentum term.[24] Labels e and h denote the electron and hole states. The band gap is associated with the $X_1$ transition, centered at 626 nm.

Photoluminescence (PL) spectra are shown in Figure 1b when the sample film is excited with 250 fs pulses, centered at 515 nm. The PL intensity is recorded for different pump pulse energies (see legend). At a low excitation pulse energy of 0.52 µJ, the exciton emission is centered at 640 nm (indicated by the dashed line labeled X). At higher pulse energies, a second peak appears at slightly shorter wavelengths, originating from amplified spontaneous emission (ASE) arising from biexciton emission (XX).[25–28] The onset of ASE is further confirmed by the superlinear dependence of the PL intensity on the pump energy[29] as shown in Figure S1 in Supporting Information. When a biexciton is annihilated, it decomposes into a photon and a single exciton $E_{XX} \rightarrow \hbar\omega + E_X$, wherein the energy of the photon $\hbar\omega = E_X - E_b$ differs from the exciton energy by the biexciton binding energy $E_b$. Thus, the wavelength shift corresponds to the biexciton binding energy $E_b = 2E_X - E_{XX}$, with $E_{XX}$ as the biexciton energy and $E_X$ the exciton energy.[30] The amount and sign of $E_b$ allows to infer the band alignment of the core/shell structure. The electrons and holes can be either confined in one region (attractive exciton–exciton interaction, $E_b > 0$), or separated between the core and the shell material (repulsive interaction, $E_b < 0$). For the former case, the QDs are called Type-I nanocrystals, while the latter corresponds to Type-II band alignment.[31] If the electrons are delocalized within the entire QD while the hole states are confined in the core material, neither exciton–exciton repulsion nor attraction is supported. The sample exhibits a border-line band structure of Type-II, referred to as quasi Type-II band alignment.[27,32] It strongly reduces the confinement of the electron and allows it to penetrate the shell. The band offset for the hole in CdSe/CdS is always positive (0.31–0.48 eV), which implicates that the hole is always localized in the CdSe core. In contrast, the reported band offset of the electron varies from −0.25 to +0.27 eV in dependence on the morphology, crystal structure of CdSe and CdS, core and shell dimension, and resulting stress or strain on the crystal lattice.[33] The biexciton emission presented in Figure 1b reveals a small blue shift of −8.5 meV with respect to the single exciton emission, indicating a quasi Type-II energy band structure.

### 2.2. THz Waveform Sensitive Electro-Absorption

We first examine THz field induced changes to the transmission of a probe pulse centered at 622 nm, corresponding to a photon energy larger than the band gap. When the THz and probe pulses spatially and temporally overlap, the QDs exhibit reduced absorption, leading to a negative change in optical density. The intense THz pulse is generated by optical rectification of mid-IR fs-pulses in the organic crystal DAST (4-*N*,*N*-dimethylamino 4′-*N*′-methyl-stilbazolium tosylate) with a repetition rate of 20 Hz, as previously reported in ref. [34] Details on the pulse characterization are found in the Experimental Section and in Supporting Information (Section S3). A THz field transient measured with electro-optic sampling (EOS) and the corresponding THz spectrum are shown in **Figure 2**a, with a peak intensity at 1.9 THz and spectral bandwidth of 2.5 THz at full-width half-maximum. By taking into account the THz pulse energy of 8.14 µJ, measured with a calibrated pyroelectric detector, and a beam radius of ~110 µm at $1/e^2$ level, measured with the knife-edge method, the maximum THz field strength at the focus position is evaluated to exceed 10 MV cm$^{-1}$. Note that, the electric field felt by the QD is substantially smaller than the applied electric field due to reflection losses and dielectric screening, as it is described in Supporting Information (Section S2). If not stated otherwise, the THz field strengths specified within this manuscript correspond to the incident THz electric field at the focal position. The blue area in Figure 2b represents the square of the THz field amplitude. The red line is the THz induced change in transmission of the QDs sample, which evidently follows the THz electric field dynamics, demonstrating the feasibility of ultrafast spectral manipulation in a sub-ps time scale and consequently the possibility of an all-optical EA modulator with data rates in the range of Tbit s$^{-1}$. However, when the THz field crosses zero, the normalized change in transmission does not reach zero. The maximum contrast between the ON–OFF signal is around 50%. In analogy to optical transmitters used for digital communication, wherein the extinction ratio is defined as the ratio between the energy (power) used to transmit a logic level "1" and energy used to transmit a logic level "0," a modulation contrast of 50% corresponds to an extinction ratio of 3 dB. The relatively small contrast is fundamentally limited by the duration and spectral width of the probe pulse. In principle, one might expect that the contrast could be improved by utilizing shorter probe pulses. However, in practice, shorter pulses lead to a broader spectrum containing spectral components above and below the QD band edge, hereby covering electro-absorption modulations of opposite sign and hence, eventually diminishing the modulation contrast. In turn, a narrow probe spectrum results in a longer pulse duration and therefore smears the time resolution. Thus, the modulation speed can be increased at the expense of the modulation contrast, and vice versa. In order to shape the THz field and elongate the oscillation period, a long pass filter with a cut-off frequency at 2 THz (Swiss Terahertz LLC) is inserted into the THz path. The resulting THz field and intensity spectrum are shown in Figure 2c. Because a fraction of the spectrum of the THz pulse is lost, the maximum incident THz field drops down to ~5.5 MV cm$^{-1}$, causing an inferior signal-to-noise ratio of the measured QD signal (see Figure 2d). However, the contrast between the THz periods is substantially increased, leading to an extinction ratio of 6.8 dB, which is comparable with that of quantum-well electro-absorption modulators operating in the GHz range.

### 2.3. Dependence on the THz Field Strength

Pein and coworkers[12] reported that above threshold THz field-induced luminescence of QDs indicates the existence of charged states which persist for longer than 1 ps.[13] As a consequence, modulation of the absorption spectrum could be temporally smeared by such longer-lived QD states. To assure that

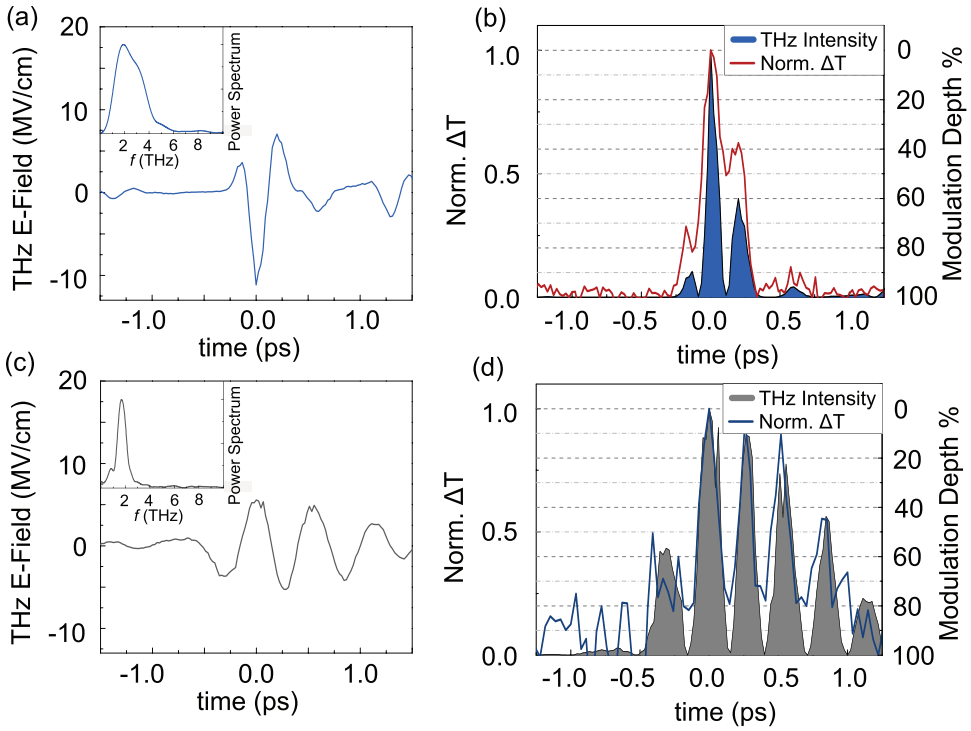


**Figure 2.** a) THz-field transient and calculated corresponding spectrum (inset). Satellite pulses at around ±1.3 ps originate from the surface reflections at the EOS crystal. b) Normalized change in transmission of the QD sample at 622 nm (red line) and THz intensity (blue area), obtained by taking a square of the field transient shown in (a). The right *y*-axis indicates the modulation depth. c,d) present the same as (a) and (b), respectively, but with a long pass filter having a cut-off frequency of 2 THz inserted into the THz path.

the poor modulation contrast in the case of a high frequency THz field is caused by the short THz period, rather than the strong electric field (which can potentially lead to the appearance of charged states), we repeat the experiment for different THz field strengths in the case of the THz transient shown in Figure 2a. The 3D plot constructed from normalized pump–probe signals (see **Figure 3**a), demonstrates that the shape of the QD response does not change significantly with the applied field strength. This reveals an absence of additional field dependent dynamics and illustrates that the modulation of the absorption spectrum originates solely from THz induced electro-absorption effects, corresponding to changes in oscillator strength, as well as the position and the width of the absorption spectrum. Moreover, the magnitude of change in absorption, given by the lock-in signal in mV (see Experimental Section), exhibits a quadratic dependence on the incident THz field (see Figure 3b), as it is expected in the case of the QCSE, and rules out field ionization mechanisms.[35]

When we assign the acquired signal from the lock-in amplifier to a certain change in the sample transmission, as described in Supporting Information, we find a 8.8% change in transmission, corresponding to ~37 mOD optical density change, when

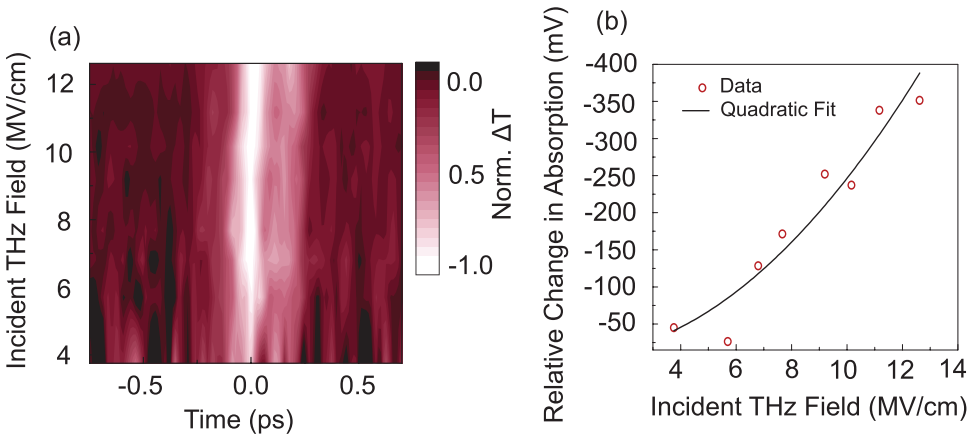


**Figure 3.** a) 3D plot of the normalized absorption changes at 622 nm for different strengths of the incident electric field. b) Peak amplitudes of the change in absorption, expressed in terms of the detected Lock In signal in mV, with respect to the incident electric field.

the probe pulse, centered at 622 nm, temporally overlaps with the maximum of an applied THz field of 10.2 MV cm$^{-1}$. Measurements with a THz field strength of 13.3 MV cm$^{-1}$ reveals a change in transmission of groundbreaking 15.8% (optical density changes of ~64 mOD), which confirms the quadratic dependence of the absorption changes on the incident THz electric field strength in Figure 3b. Although similar changes of ~50 mOD were reported in the case of the optical Stark effect in CdSe colloidal quantum wells, driven by 170 fs, 730-nm pulses,[36] to the best of our knowledge, our results represent the highest value of electro-absorption modulation by intense THz radiation ever reported for solution processed materials at room temperature.

### 2.4. Analysis of Electro-Absorption Spectra

Finally, we qualitatively discuss the QCSE by analyzing pump-probe spectra measured by tuning the central wavelength of the probe pulse across the band gap of the QD film , as it is illustrated in **Figure 4**a. For each central wavelength, we sample the THz induced change in transmission with respect to the time delay between the THz pump and visible probe pulse, and evaluate a change in optical density with the time integrated signal of the resulting transmission modulation transients. The results of two separate measurements with different field strengths are presented in Figure 4b by green and red dots. In order to identify the origin of the THz induced modulation of the absorption spectrum, we perform simulations on the underlying modifications of the electronic states in the case of various energy band structures.

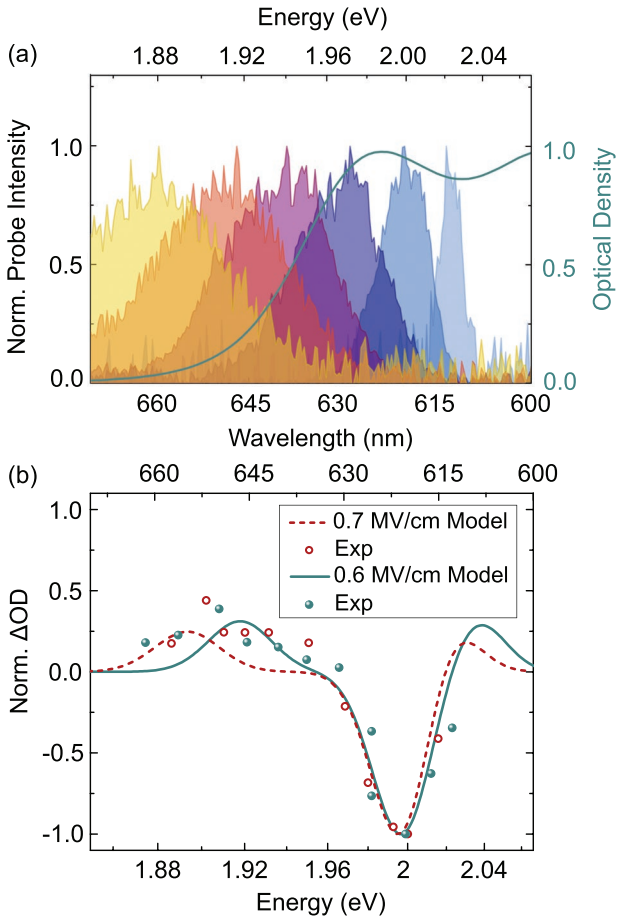


**Figure 4.** a) Optical density (green line) and normalized probe spectra (areas) tuned across the band edge. b) Measured Stark spectra (dots) for two different field strengths experienced by the excitons, and simulated changes in optical density (lines) for 0.7 (red) and 0.6 MV cm$^{-1}$ (green).

In analogy to electro-absorption spectroscopy (also known as Stark spectroscopy), the optical density can be described with respect to the optical frequency $\nu$ as

$$OD(\nu)/\nu \sim |\mu_{vc}|^2 s(\nu) \quad (1)$$

with the electric transition dipole moment $\mu_{vc} = e\langle \Psi_v | \hat{r} | \Psi_c \rangle$ from valance band state $|\Psi_v\rangle$ to conduction band state $|\Psi_c\rangle$, fundamental electric charge $e$, position state operator $\hat{r}$ and normalized line shape function $s(\nu)$.[37–39] In the presence of an external electric field $F$ the absorption spectrum can be expressed as

$$OD^F(\nu)/\nu \sim |\mu_{vc}^F|^2 s^F(\nu) \quad (2)$$

In the case when the line shape function does not change significantly under the influence of the external field, it can be approximated by $s^F(\nu) \approx s(\nu - \nu_{st})$, with $h\nu_{st}$ being the Stark energy shift,[37] accounting for the energy shift of the electronic levels when an external electric field is applied. The change in absorption amplitude is mainly caused by the altered transition dipole moment $\mu_{vc}^F$ which is dominated by the overlap integral of electron and hole wavefunctions $\varphi_e|\varphi_h$.[40,41]

Stark spectroscopy was originally applied to an ensemble of molecules, where field-induced alignment/orientation is possible. However, to date it is also successfully utilized on confined structures, such as layered hybrid perovskites[19] or CdSe nanocrystals,[35] where orientational effects are unlikely since the films are rigid. The principal requirement for the validity of the Stark formalism is that the electronic states of the system are discrete,[35] as they are in QD structures. When Liptay first theoretically formulated Stark spectroscopy,[37] he used perturbation theory to account for the change in transition dipole moment as well as for the energy shift. However, when the applied electric fields are in the MV cm$^{-1}$ range, which is the case of this particular work, the assumption of small perturbations is not valid anymore. For the case of strong electric fields, Pein et al.[13] used an elaborate full-atomic, semi-empirical tight binding model in order to describe the electron and hole states. Here, we exploit an effective 1D approach to obtain envelope wave functions. Despite the simplified concept, our calculations reproduce the results from Pein and coworkers surprisingly well, emulate Liptay's model for small fields and provide a qualitative insight into the physical behavior of the QDs. A detailed description of the theoretical model used for the calculations is given in the Supporting Information (Section S4). Here, we highlight main assumptions and considerations. First of all, due to the strong confinement, an individual Hamiltonian for electrons and holes is sufficient to describe excitons.[42] Second, in the model, the energy surface of the CdSe/CdS heterostructure is introduced as a step-like external potential, and

an effective Hartree operator, caused by the Coulomb potential, is used to describe interactions. The external electric field is introduced by $\hat{V}_F = \pm eFz$, where $F$ denotes the applied electric field along the $z$-direction. Although the energy states of this model reproduce the measured ones within a few percent, in order to improve comparability, a small shift was added. Because optical properties are very sensitive to the quantum dot parameters, as well as to the dielectric environment originating from surrounding ligands,[43–45] such a slight shift can be justified. Finally, the higher-energy transitions were not included in the model based on their negligible contribution in the probed spectral range, due to both higher energy and the inverse dependence of the transition dipole moment on the energy gap.

Measured and simulated Stark spectra are depicted in Figure 4b for two different THz field strengths acting on the QDs. In order to compare the results of the measurements and the calculations, the spectra are normalized. The two sets of experimental data presented in Figure 4b are fitted by varying the strength of the electric field experienced by the QDs. The best match between experiment and theoretical model are found for an electric field strength between 0.6 (green) and 0.7 MV cm$^{-1}$ (red) (for details see Supporting Information). The negative optical density changes around 2 eV are attributed to a reduction of the normalized overlap integral at the band gap with respect to the overlap integral of the unperturbed QD. According to the simulations, the induced positive optical density changes on the red side of the pump–probe spectrum (1.87 eV–1.95 eV) originate from a red shift of the first transition energy (denoted as $X_1$ in Figure 1a). Spectral broadening of the transition is not taken into account in the model. The positive change in optical density on the blue side of the energy band gap (> 2.02 eV) is caused by the transition $1P_{3/2}(h) \rightarrow 1S(e)$, which is originally forbidden when no external field is applied due to the symmetry of the wave-functions. The applied electric field breaks the symmetry and increases the absorption for shorter wavelengths. Unfortunately, the blue spectral range cannot be experimentally resolved due to the limited tunability of the probe pulse (610–800 nm). In the case of stronger electric fields (> 0.8 MV cm$^{-1}$), both transitions are shifted to even longer wavelengths, such that no changes in optical density can be observed on the blue side of the energy band gap, as discussed in Supporting Information. A discrepancy between the calculated and the measured data at lower photon energies is attributed to the broad spectrum and finite pulse duration of the probe pulse, which drastically reduces the spectral sensitivity of the central wavelength, as well as intensity fluctuations. Although a full 3D model would improve the accuracy of the calculated energy states, a sufficiently good overlap between the measured data and simulations validates the simple model and justifies further discussions on the energy band structure.

**Figure 5** shows the square of the overlap integral, its relative change, as well as the Stark shift with respect to the applied electric field, simulated for three types of band alignments. As it follows from the simulations, the strongest change of the overlap integral and the largest Stark shift, especially at small and moderate electric field strengths, is expected for Type-II and quasi Type-II band structures, when the relatively loosely confined de-localized electrons travel the furthest possible distance

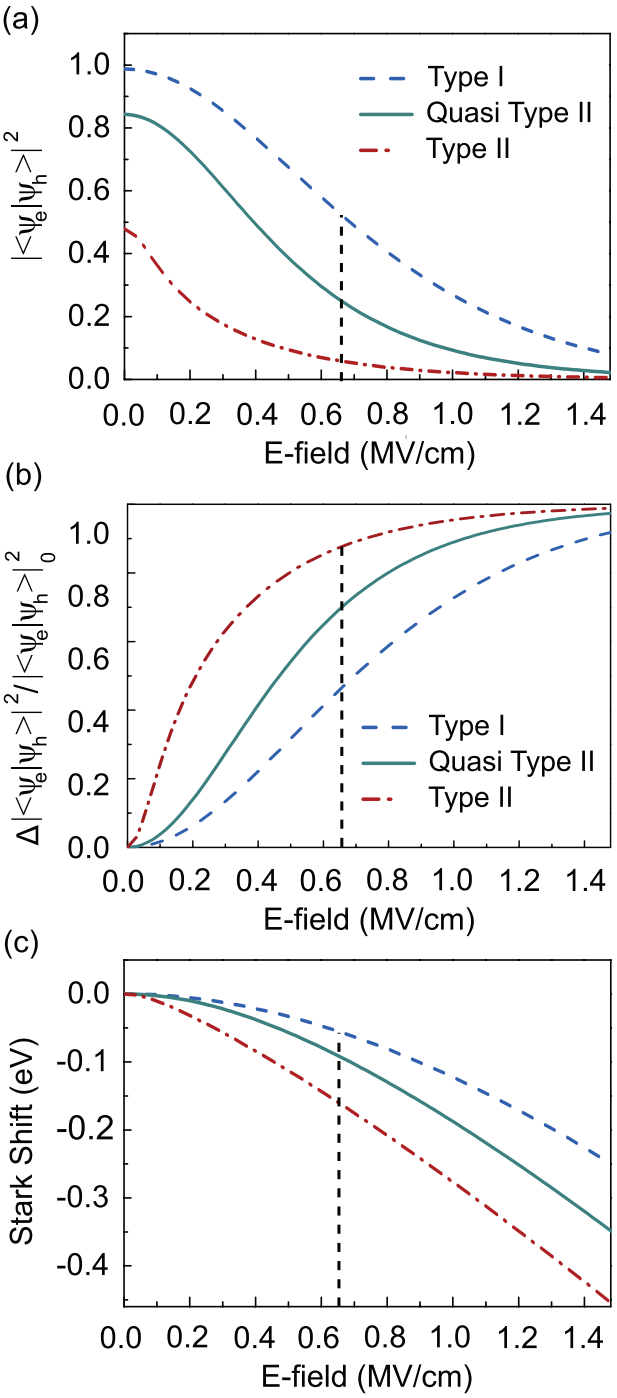


**Figure 5.** a) Calculated square of the overlap integral of the electron and hole wavefunction, and b) relative change as a function of the electric field strength for three different energy band alignments (see legend). c) Stark shift for different electric field strengths. Dashed vertical lines indicate a field strength of 0.65 MV cm$^{-1}$, which is relevant to the data presented in Figure 4b.

away from the holes, leading to a large spatial separation of both charge carriers. Our findings are further supported by observations from Bozyigit et al.,[46] who attributed PL quenching in colloidal CdSe/CdS QDs to the spatial separation of electron

and hole wave-functions (causing the optical transition matrix element to decrease), rather than to the field induced charging of the QDs. Largest reduction of the PL in ref. [46] was observed for QD band structures with relaxed confinement potentials, wherein the reduced band offset of the conduction band at the core/shell-interface allows a strong separation of the electron and hole.

Although the relative changes are similar for Type-II and quasi Type-II in the case of strong electric fields exceeding 1 MV $cm^{-1}$, a Type-II energy band alignment reaches significantly larger values for smaller electric fields, as depicted in Figure 5b. Such a band structure can be attained with a very thick shell, which allows the electrons to delocalize freely over the entire QD volume, while the holes are confined in the core.[27] Accordingly, the separation between electron and hole wavefunctions becomes even more pronounced for thicker shells due to the reduced confinement of the electron. Thus, for an absorption spectrum with sharp and well pronounced features, a Type-II structure can be beneficial since small fields can lead to large energy shifts, in addition to a reduced overlap integral, resulting in a drastic change in absorption. However, although it was predicted by simulations[47,48] that the magnitude of the QCSE shifts of the electron and hole levels increase monotonically with the well width in quantum well structures, an upper limit on the scalability of the QCSE is given by the exciton Bohr radius.[5] Increasing the width of nano-devices diminishes the quantum confinement and reduces the exciton binding energy, such that the exciton eventually field-ionizes and the bulk electric field response would be expected.

## 3. Conclusion

In summary, we demonstrate a route for direct THz induced sub-ps modulation of the optical density in colloidal CdSe/CdS QDs in the visible spectral range, at room temperature, without any field enhancing structures, and with an extreme change in transmission of 15%. The modulation shape and depth can be controlled by the shape of the THz transient and leads to an extinction ratio exceeding 6 dB at a potential data rate in the Tbit $s^{-1}$ range. The fact that we can access the QCSE directly without field enhancing structures, allows us to study a large variety of samples and excludes possible artifacts from the enhancement structure. Supported by theoretical simulations, we attribute the large Stark signal to a significant change of the overlap integral promoted by the beneficial band alignment of the CdSe/CdS quantum dots, originating from the small conduction band offset between the core/shell interface. We further suggest that Type II QDs are promising materials for EA modulators with extremely high modulation signals. The fact that CdSe/CdS QDs can be tuned between the Type-I and Type-II regime by varying the core radius and shell thickness,[27,29] makes it possible to precisely adjust the energy band structure. The possibility to further tune the absorption spectrum of QDs from the visible to the telecommunication wavelength by an appropriate choice of composition, size and barrier width, along with their solution processability makes them excellent candidates for applications in high-speed optical communication systems.

## 4. Experimental Section

*THz Pulse Generation and Characterization*: The experimental setup resembles a conventional electro-optic sampling arrangement (see Figure S2, Supporting Information). THz radiation was generated in the organic crystal DAST by optical rectification of high-energy mid-IR pulses centered at 3.9 µm, from an optical parametric chirped pulse amplifier (OPCPA). Details on the generation scheme are reported in ref. [34] For the characterization of the generated THz pulse, THz radiation was seperated from the mid-IR pump with several long pass filters and focused on a 50 µm thick GaP crystal. The probe pulse was generated in a white light seeded non-collinearly pumped optical parametric amplifier, producing shorter than 50 fs pulses with a tunable central wavelength from 610 to 850 nm. The intensity of the probe pulse was controlled with a variable neutral density filter. After the EOS crystal, the probe was steered through a quarter wavelength retardation plate (QWP) and a Wollaston prism (WP). The THz induced change in polarization with respect to the position of the delay stage was detected with a balanced detector, consisting of two photo diodes labeled PD A and PD B. The output of the mid-IR OPCPA was chopped at 10 Hz with an optical chopper which was synchronized with the laser system. The repetition rate of the chopper further provided the trigger to the lock-in amplifier, which registered a difference between the signals from PD A and PD B. A boxcar integrator was installed in-between the balanced detector and the lock-in to further reduce noise and amplify the detectable signal.[49]

*THz-Pump Visible-Probe Setup*: In order to measure THz-induced changes in transmission of the probe pulse, the CdSe/CdS QD sample was placed at the position of the GaP crystal. The setup was slightly reconfigured by intercepting the probe beam after the sample with a flip mirror to avoid propagation through the QWP and WP (see Figure S2, Supporting Information). In addition, a fraction of the probe beam was reflected with a beam splitter before the sample and used as a reference beam. It was steered to PD A for the reduction of noise originating from intensity fluctuations. In the absence of THz radiation, the signal on the detector was balanced with a variable attenuator made of a Glan–Taylor polarizer and a half waveplate, installed before the detector PD A. To reduce THz absorption by water molecules in ambient air, the whole setup was purged with nitrogen, resulting in <3% relative humidity.

Assignment of the measured signal to absolute changes in transmission was performed via a calibration procedure involving electro-optic modulation of a reference beam with a known modulation amplitude and measurement of the resulting signal with a lock-in amplifier (for details see Section S3, Supporting Information).

## Supporting Information

Supporting Information is available from the Wiley Online Library or from the author.

## Acknowledgements

This project was funded by the European Union's Horizon 2020 program, through a FET Open research and innovation action (Grant No. 899141 PoLLoC), by the Austrian Science Fund (Grant No. I 4566), Hochschuljubiläumsfond der Stadt Wien (Grant No. H-260733/2020), and Österreichische Forschungsförderungsgesellschaft (Grant 871934).

## Conflict of Interest

The authors declare no conflict of interest.

## Data Availability Statement

The data that support the findings of this study are available in supplementary material of this article.

## Keywords

colloidal quantum dots, high-speed optical communication systems, nano-device technology, nonlinear THz spectroscopy, THz induced Stark effect in confined structures, ultrafast electro absorption switching

Received: November 5, 2021
Revised: January 24, 2022
Published online: March 3, 2022

[1] R. Kirchain, L. Kimerling, *Nat. Photonics* **2007**, *1*, 303.
[2] G. T. Reed, G. Mashanovich, F. Y. Gardes, D. J. Thomson, *Nat. Photonics* **2010**, *4*, 518.
[3] Y.-H. Kuo, Y. K. Lee, Y. Ge, S. Ren, J. E. Roth, T. I. Kamins, D. A. B. Miller, J. S. Harris, *Nature* **2005**, *437*, 1334.
[4] D. A. B. Miller, D. S. Chemla, T. C. Damen, A. C. Gossard, W. Wiegmann, T. H. Wood, C. A. Burrus, *Phys. Rev. Lett.* **1984**, *53*, 2173.
[5] D. A. B. Miller, D. S. Chemla, T. C. Damen, A. C. Gossard, W. Wiegmann, T. H. Wood, C. A. Burrus, *Phys. Rev. B* **1985**, *32*, 1043.
[6] D. A. B. Miller, D. S. Chemla, S. Schmitt-Rink, *Phys. Rev. B* **1986**, *33*, 6976.
[7] P. Chaisakul, D. Marris-Morini, M.-S. Rouifed, G. Isella, D. Chrastina, J. Frigerio, X. L. Roux, S. Edmond, J.-R. Coudevylle, L. Vivien, *Opt. Express* **2012**, *20*, 3219.
[8] H. Fukano, T. Yamanaka, M. Tamura, *J. Lightwave Technol.* **2007**, *25*, 1961.
[9] M. Stepanenko, I. Kulinich, I. Yunusov, *J. Phys.: Conf. Ser.* **2019**, *1145*, 012028.
[10] J. Federici, L. Moeller, *J. Appl. Phys.* **2010**, *107*, 111101.
[11] M. C. Hoffmann, B. S. Monozon, D. Livshits, E. U. Rafailov, D. Turchinovich, *Appl. Phys. Lett.* **2010**, *97*, 231108.
[12] B. C. Pein, W. Chang, H. Y. Hwang, J. Scherer, I. Coropceanu, X. Zhao, X. Zhang, V. Bulović, M. Bawendi, K. A. Nelson, *Nano Lett.* **2017**, *17*, 5375.
[13] B. C. Pein, C. K. Lee, L. Shi, J. Shi, W. Chang, H. Y. Hwang, J. Scherer, I. Coropceanu, X. Zhao, X. Zhang, V. Bulović, M. G. Bawendi, A. P. Willard, K. A. Nelson, *Nano Lett.* **2019**, *19*, 8125.
[14] A. Sell, A. Leitenstorfer, R. Huber, *Opt. Lett.* **2008**, *33*, 2767.
[15] K. Reimann, R. P. Smith, A. M. Weiner, T. Elsaesser, M. Woerner, *Opt. Lett.* **2003**, *28*, 471.
[16] H. Hirori, A. Doi, F. Blanchard, K. Tanaka, *Appl. Phys. Lett.* **2011**, *98*, 091106.
[17] C. Vicario, B. Monoszlai, C. P. Hauri, *Phys. Rev. Lett.* **2014**, *112*, 213901.
[18] A. D. Koulouklidis, C. Gollner, V. Shumakova, V. Y. Fedorov, A. Pugžlys, A. Baltuška, S. Tzortzakis, *Nat. Commun.* **2020**, *11*, 292.
[19] G. Walters, M. Wei, O. Voznyy, R. Quintero-Bermudez, A. Kiani, D. Smilgies, R. Munir, A. Amassian, S. Hoogland, E. Sargent, *Nat. Commun.* **2018**, *9*, 4214.
[20] Y. D. Sibirmovsky, N. I. Kargin, I. S. Vasil'evskii, in *2019 PhotonIcs Electromagnetics Research Symposium - Spring (PIERS-Spring)*, IEEE, Piscataway, NJ **2019**, pp. 733–740.
[21] O. Chen, J. Zhao, V. P. Chauhan, J. Cui, C. Wong, D. K. Harris, H. Wei, H.-S. Han, D. Fukumura, R. K. Jain, M. G. Bawendi, *Nat. Mater.* **2013**, *12*, 445.
[22] Norris , Bawendi, *Phys. Rev. B, Condens. Matter* **1996**, *53*, 16338.
[23] C. Zhang, T. N. Do, X. Ong, Y. Chan, H.-S. Tan, *Chem. Phys.* **2016**, *481*, 157.
[24] J. R. Caram, H. Zheng, P. D. Dahlberg, B. S. Rolczynski, G. B. Griffin, D. S. Dolzhnikov, D. V. Talapin, G. S. Engel, *J. Chem. Phys.* **2014**, *140*, 084701.
[25] V. I. Klimov, A. A. Mikhailovsky, S. Xu, A. Malko, J. A. Hollingsworth, C. A. Leatherdale, H.-J. Eisler, M. G. Bawendi, *Science* **2000**, *290*, 314.
[26] A. Polovitsyn, A. H. Khan, I. Angeloni, J. Q. Grim, J. Planelles, J. I. Climente, I. Moreels, *ACS Photonics* **2018**, *5*, 4561.
[27] A. F. Cihan, Y. Kelestemur, B. Guzelturk, O. Yerli, U. Kurum, H. G. Yaglioglu, A. Elmali, H. V. Demir, *J. Phys. Chem. Lett.* **2013**, *4*, 4146.
[28] C. Gollner, J. Ziegler, L. Protesescu, D. N. Dirin, R. T. Lechner, G. Fritz-Popovski, M. Sytnyk, S. Yakunin, S. Rotter, A. A. Yousefi Amin, C. Vidal, C. Hrelescu, T. A. Klar, M. V. Kovalenko, W. Heiss, *ACS Nano* **2015**, *9*, 9792.
[29] L. Dong, A. Sugunan, J. Hu, S. Zhou, S. Li, S. Popov, M. S. Toprak, A. T. Friberg, M. Muhammed, *Appl. Opt.* **2013**, *52*, 105.
[30] V. I. Klimov, *Annu. Rev. Phys. Chem.* **2007**, *58*, 635.
[31] A. Piryatinski, S. A. Ivanov, S. Tretiak, V. I. Klimov, *Nano Lett.* **2007**, *7*, 108, pMID: 17212448.
[32] R. Mastria, A. Rizzo, *J. Mater. Chem. C* **2016**, *4*, 6430.
[33] D. Steiner, D. Dorfs, U. Banin, F. Della Sala, L. Manna, O. Millo, *Nano Lett.* **2008**, *8*, 2954.
[34] C. Gollner, M. Shalaby, C. Brodeur, I. Astrauskas, R. Jutas, E. Constable, L. Bergen, A. Baltuška, A. Pugžlys, *APL Photonics* **2021**, *6*, 046105.
[35] V. L. Colvin, K. L. Cunningham, A. P. Alivisatos, *J. Chem. Phys.* **1994**, *101*, 7122.
[36] B. T. Diroll, *Nano Lett.* **2020**, *20*, 7889.
[37] W. Liptay, J. Czekalla, *Z. Naturforsch. A* **1960**, *15*, 1072.
[38] W. Liptay, *Ber. Bunsenges. Phys. Chem.* **1976**, *80*, 207.
[39] W. Liptay, *Angew. Chem., Int. Ed.* **1969**, *8*, 177.
[40] E. O. Kane, *J. Phys. Chem. Solids* **1958**, *6*, 236.
[41] Y. Peter, M. Cardona, *Fundamentals of Semiconductors: Physics and Materials Properties*, Springer, Berlin, Heidelberg **2010**.
[42] E. Tyrrell, J. Smith, *Phys. Rev. B* **2011**, *84*, 165328.
[43] A. Nazzal, H. Fu, *J. Comput. Theor. Nanosci.* **2009**, *6*, 1277.
[44] J. Casas Espínola, X. Hernández Contreras, *J. Mater. Sci.: Mater. Electron.* **2017**, *28*, 10.
[45] N. Zeiri, A. Naifar, S. Abdi-Ben Nasrallah, M. Said, *Results Phys.* **2019**, *15*, 102661.
[46] D. Bozyigit, O. Yarema, V. Wood, *Adv. Funct. Mater.* **2013**, *23*, 3024.
[47] M. Matsuura, T. Kamizato, *Phys. Rev. B* **1986**, *33*, 8385.
[48] T. Hiroshima, R. Lang, *Appl. Phys. Lett.* **1986**, *49*, 639.
[49] D. P. Khatua, S. Gurung, A. Singh, S. Khan, T. K. Sharma, J. Jayabalan, *Rev. Sci. Instrum.* **2020**, *91*, 103901.